2023 8th International Conference on
Advanced Robotics and Mechatronics
July 8-10, Sanya, China

A Graph-Based SLAM Method Assisted by Visual Marker in the Degenerate Scenes

Jieqingxin Zhang[1], Hui Zhang[2], Xidong Zhou[1], Bo Chen[2], Xiangchuan Wang[1] and Tao Xu[3]

Abstract— **In the post-COVID-19 pandemic era, hospitals and other places have an urgent need for mobile robots with autonomous disinfection ability, and robots need to complete SLAM tasks to realize autonomous navigation. Lidar is widely used for indoor SLAM. However, due to the lack of geometric structure in the indoor environment, two-dimensional lidar information degrades, rendering the robot unable to obtain effective positioning. Therefore, we leverage the easy identification and high robustness of ARTag to fuse vision and range sensor information. We introduce ARTag as visual marker to assist positioning, establish observation window to screen the acquired ARTag pose. We employ the pose graph optimization method to optimize the visual markers and laser scanning results in the back end. This reduces the positioning errors caused by the degradation of lidar information and reduces the frequency of optimization by improving the back end optimization strategy. This method is applied in a UltraViolet C (UVC) Disinfection Robot experiment. Experimental results show that our method effectively improves the positioning accuracy and robustness of the robot in the environments with degraded laser information.**

I. INTRODUCTION

In the post-COVID-19 pandemic era, large-scale human infections has a great impact on social production efficiency. Hospitals and other places are in urgent need of equipment with long-term autonomous disinfection ability. We proposed and designed an intelligent disinfection robot. In order to complete the disinfection task autonomously, the robot needs to build an accurate map and find its position in the map in real time, which constitutes a Simultaneous Localization and Mapping (SLAM) problem [1].

This work was supported in part by the National Key RD Program of China under Grant 2021ZD0114503, the Major Research plan of the National Natural Science Foundation of China (Grant No. 92148204), the National Natural Science Foundation of China under Grants 62027810, 61971071, 62133005, Hunan Leading Talent of Technological Innovation under Grant 2022RC3063, Hunan Science Fund for Distinguished Young Scholars under Grant 2021JJ10025, Hunan Key Research and Development Program under Grants 2021GK4011,2022GK2011, Chang sha Science and Technology Major Project under Grant kh2003026, Joint Open Foundation of state Key Laboratory of Robotics under Grant 2021-KF-22-17, China University industry-University-research Innovation Fund under Grant 2020HYA06006.

[1]Jieqingxin Zhang, Xidong Zhou and Xiangchuan Wang are with the College of Electrical and Information Engineering, Changsha University of Science and Tech-nology, Hunan, China e-mail: 1337503837@qq.com; 741170053@qq.com; wxcwxc200087@163.com

[2]Hui Zhang and Bo Chen are with College of Robotics, also with Robot Visual Perception and Control Technology National Engineering Research Center, Hunan University, Hunan, China e-mail: zhanghuihby@126.com; cb233cb@163.com

[3]Tao Xu is with College of Electrical and Information Engineering, Hunan University, Hunan, China e-mail: xutao1998.@hnu.edu.cn

Gmapping [2], Hector [3] and Cartographer [4] are the most widely used SLAM methods, where, Grisetti G et al. [2] proposed an improved SLAM algorithm based on particle filtering (PF), it is not suitable for application in the large environment due to the huge computing amount brought by the increasing number of particles. Kohlbrecher et al. [3] proposed the Gauss Newton optimization method for scan-matching and realized SLAM without odometry, but this method is not suitable for indoor low cost requirements. Konolige K et al. [5] proposed a method called sparse pose adjustment (SPA), which solved the bottleneck problem of nonlinear optimization. Hess W et al. [4] use a branch-and-bound approach for computing scan-to-submap matches as constraints, it reduces the calculation of loop-closure and Cartographer becomes one of the most mainstream indoor SLAM algorithms. However, Cartographer in an environment where the sensor information is degraded, due to insufficient effective constraints, positioning becomes difficult, and incorrect positioning results will bring disastrous impact on subsequent SLAM tasks [6].

The degradation of distance sensor often occurs in the environment of lack of geometric structure, such as corridor. When a robot carrying lidar passes through the corridor, it can be located to multiple positions with similar characteristics, which will make the robot's positioning constantly jump and seriously affect the robot's navigation. In order to overcome information degradation, Zhang J et al. [7] searched for the direction of lidar information degradation, but only partially solved the problem in the direction of good conditions. Multi-sensor fusion is often used as a solution to information degradation [8]. Patrick Geneva et al. [9] used extended Kalman filter (EKF) for multi-sensor fusion to develop a more accurate positioning system than Cartographer. Y. Deng et al. [10] used Global Positioning System (GPS) and lidar fusion. Robust positioning is obtained outdoors, but indoor occlusion makes GPS less effective. Zhen W et al. [11] used error state Kalman filter (ESKF) fusion inertial measurement unit (IMU) to solve Lidar degradation, but this method cannot effectively solve the cumulative error. Scherer S et al. [12] fused radar and ultra wide band (UWB) to achieve robust positioning in tunnel, Xin J et al. [13] use PF combined with UWB to improve accuracy, but both methods require the prior pose of UWB.

In this paper, based on the Cartographer framework, a similar scheme is used for fusion with visual sensors, However, due to the particularity of the indoor environment, the wall texture characteristics of a single, usually visual sensor is easy degenerate in the lack of texture features

2023 International Conference on Advanced Robotics and Mechatronics (ICARM) | 979-8-3503-0017-8/23/$31.00 ©2023 IEEE | DOI: 10.1109/ICARM58088.2023.10218772

Authorized licensed use limited to: HUNAN UNIVERSITY. Downloaded on April 09,2024 at 11:14:45 UTC from IEEE Xplore. Restrictions apply.

environment [1], and the ordinary visual sensor fusion is difficult to solve the wrong positioning of the indoor corridor. Therefore, ARTag is used to supplement texture information to prevent degradation of visual sensors, and the pose of visual markers on the map can be obtained by a graph-based optimization method during mapping, rather than by manual measurement after layout. The main contributions of this paper are as follows:

1. The method is proposed to using ARTag as visual marker to assist lidar localization and mapping in indoor degenerate scenes.

2. The ARTag pose as a landmark was processed by establishing an observation window.

3. Improved the back-end optimization strategy of Cartographer, and performing pure localization when using landmark constraints substantially reduces the global optimization frequency.

II. SYSTEM OVERVIEW

The overall framework of system SLAM is shown in the Fig. 1. Encoders, lidar, IMU and cameras are used as sensor inputs. In the environment of lidar information degradation, visual markers are used to assist positioning, and accurate map and precise positioning of robots in the map are output.

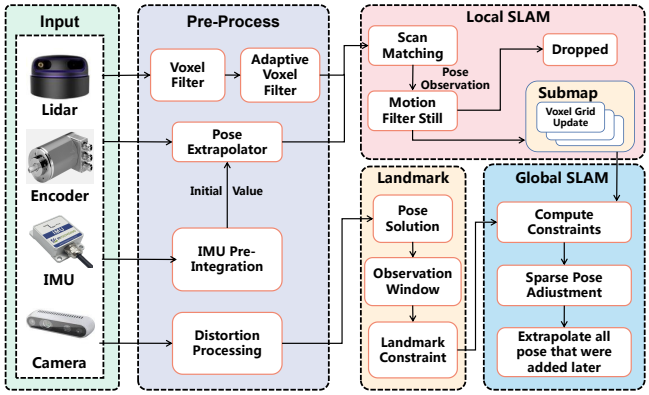

Fig. 1. Overall system framework

In the pro-process module, the encoder is mainly used as pose extrapolator, and the IMU provides the initial value for that. The point cloud obtained by the radar is output to the Local SLAM module after the voxel filtering and adaptive voxel filtering. The camera provides the image information containing ARTag, and the image distortion is eliminated, then output to the Landmark module. In the Local SLAM module, the processed point cloud combined with pose extrapolator is used for scan-matching. Scan matcher based on Ceres library will insert radar data into submap, which is an occupancy grid map. The pose $\xi = (\xi_x, \xi_y, \xi_\theta)$ of the robot at moment i is called scan. The pose of scan will be formed into Node x_i, and then motion estimation will be carried out to discard invalid scan matching results. Valid matching results will be used to construct Submap node m_i. Continuous correlated scan will form submap nodes, and a new submap will be constructed only after a submap is formed. When a new Node is created, a constraint is built between the submap closest to it. In Landmark module, the processed image information is obtained. After extracting the pose and label information of ARTag, the pose is input into the observation window for screening, and then added into the back-end optimization as landmark constraint. In Global SLAM, scan and submap obtained from Local SLAM is used to construct graph with landmark obtained from landmark module, and the graph is optimized according to SPA. Finally, the map, robot trajectory and landmark's pose in the map are output. When it comes to improvements in back-end optimization, the Landmark module and Global SLAM module are discussed in detail in Chapter III.

III. INTERGRATION OF VISUAL MARKER IN BACK-END OPTIMIZATION

In this chapter, the methods in Landmark module and Global SLAM module in the overall framework of the system are elaborated, and we introduce how to obtain landmark by using ARTag and how to improve the back-end optimization by adding landmark.

A. Visual Landmarks

ARTag visual tag library is a system with 2002 planar tags [14], each of the 2002 digits is encoded to produce a black and white rasterized image, which is easy to recognize and has strong anti-interference. Before the camera is used to obtain the pose of ARTag in the environment, the internal and external parameters of the camera need to be calibrated first [15][16].

Use the method in [17] to identify ARTags, calculate the gradient of each pixel in the image, including the amplitude and direction, and perform the cluster fitting operation to gather the pixels into components with similar gradient direction and size, then by searching the ARTag visual tag library and comparing the data, identify the number ID and the transformation matrix $T_{a,c}$ of the extracted ARTag based on the coordinate system of the camera, and decompose the matrix $T_{a,c}$ into pose $\xi_a^c = (x_a, y_a, z_a, \theta)$. θ is the rotation Angle about the X-axis of the camera coordinate system. There may be misidentification due to the above process, we set fixed window W_c and distance limits $distance_{max}$, the pose that does not meet the requirements will not be used for constraint calculation. The formula is as follows:

$$W_c = \begin{cases} x_{\min} < x_a < x_{\max} \\ y_{\min} < y_a < y_{\max} \\ 0 < z_a < distance_{max} \\ \theta_{\min} < \theta < \theta_{\max} \end{cases} \tag{1}$$

The coordinate transformation matrix $T_{a,r}$ of ARTag in the coordinate system of robot is obtained by combining with the model information of robot and $T_{s,c}$ provided by external parameters. Where $R_{a,r} \in \mathrm{SO}(2)$, $t_{a,r} \in \mathbb{R}^2$.

$$T_{a,r} = \begin{bmatrix} R_{a,r} & t_{a,r} \\ 0^T & 1 \end{bmatrix} \tag{2}$$

Authorized licensed use limited to: HUNAN UNIVERSITY. Downloaded on April 09,2024 at 11:14:45 UTC from IEEE Xplore. Restrictions apply.

B. Global SLAM

In this framework, pose graph [18] is used for back-end optimization. The basic idea of graph optimization is to abstract the pose of the robot at different moments into points, and the constraints observed by different sensors at different moments of the robot as edges. Graph-based SLAM is to take all the points and edges constructed in the process of mapping as a least squares problem. Use iteration to find the optimal solution.

Let $X=(X_1,X_2,...,X_n)^T$ be the vector of one parameter, where x_i describes the pose of i th node, $\hat{z}_{ij}$ and Ω_{ij} represent the observed measures and information matrix between nodes i and j respectively. The observed metric is a transformation, so that the attitude between different nodes can be compared uniformly. If there is no error, $\hat{z}_{ij}$ and z_{ij} will be the same, the information matrix represents the degree of trust in different observation measures, so that the observation measures of different nodes are consistent as far as possible in the case of errors, this relationship can be described by a vector error function:

$$e_{ij}\left(x_i,x_j,z_{ij}\right)=z_{ij}-\hat{z}_{ij}\left(x_i,x_j\right) \tag{3}$$

With the residual function, the problem can be easily transformed into an optimization problem, and the graph optimization is expressed as a least squares problem:

$$X^*=\operatorname{argmin}_x F(x) \tag{4}$$

$$F(x)=\sum_{\langle i,j\rangle\in C} e_{ij}^T\Omega_{ij}e_{ij} \tag{5}$$

$F(x)$ is the function to be optimized, X^* represents the parameter configuration of each node of x that minimizes the optimization function $F(x)$, and e_{ij} is the difference between the predicted observation metric $\hat{z}_{ij}$ and the actual observation metric z_{ij} of the robot.

In the Global SLAM module of this paper, as shown in Fig. 2, Node x_j and Submap m_i nodes provided by the Local SLAM module are used as points, and the constraint is shown as the coordinate transformation between x_j and m_i and its covariance matrix. landmark module adds additional node l_k and constraint ξ_{jk} to the graph, which ξ_{jk} are converted by the matrix $T_{a,r}$ in Subsection A. All x_j, m_i and l_k are optimized using graph optimization.

According to equations (3)-(5), the least squares problem of back-end optimization in Global SLAM is described as follows:

$$\underset{\Xi^m,\Xi^s,\Xi^l}{\operatorname{argmin}}\frac{1}{2}\sum_{ijk}\left(\rho\left(E^2\left(\xi_i^m,\xi_j^s,\Sigma_{ij},\xi_{ij}\right)\right)+E^2\left(\xi_k^l,\xi_j^s,\Sigma_{jk},\xi_{jk}\right)\right) \tag{6}$$

$$E^2\left(\xi_i^m,\xi_j^s,\Sigma_{ij},\xi_{ij}\right)=e\left(\xi_i^m,\xi_j^s,\xi_{ij}\right)^T{\Sigma_{ij}}^{-1}e\left(\xi_i^m,\xi_j^s,\xi_{ij}\right) \tag{7}$$

$$e\left(\xi_i^m,\xi_j^s,\xi_{ij}\right)=\xi_{ij}-\begin{pmatrix} R_{\xi_i^m}^{-1}\left(t_{\xi_i^m}-t_{\xi_j^s}\right)\\ \xi_{i;\theta}^m-\xi_{j;\theta}^s\end{pmatrix} \tag{8}$$

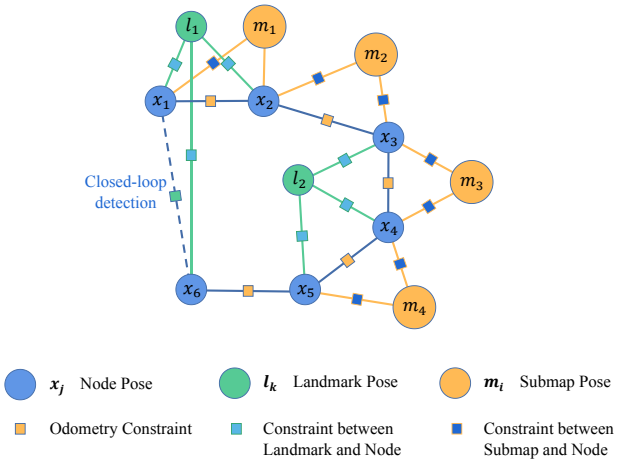

Fig. 2. Pose graph for back-end optimization

$\Xi^m=\{\xi_i^m\}_{i=1,...,\mathrm{m}}$ indicates the pose of the i th submap, $\Xi^m=\left\{\xi_j^s\right\}_{j=1,...,\mathrm{s}}$ indicates the pose of the j th scan, ξ_{ij} represents the pose of the j th scan matched in the i th submap coordinate system, Σ_{ij} is its covariance matrix, Σ_{ij} can be estimated using the multivariate Gaussian distribution fitting method [19]. ρ is a loss function used to reduce the influence of outliers. $\Xi^l=\left\{\xi_k^l\right\}_{k=1,...,\mathrm{m}}$ is the pose of the k th landmark, ξ_{jk} represents the pose of the k th landmark obtained in the j th scanning coordinate system, Σ_{jk} is its covariance matrix, among them,the vector error function of landmark is described as:

$$E^2\left(\xi_k^l,\xi_j^s,\Sigma_{jk},\xi_{jk}\right)=e\left(\xi_k^l,\xi_j^s,\xi_{jk}\right)^T{\Sigma_{jk}}^{-1}e\left(\xi_k^l,\xi_j^s,\xi_{jk}\right) \tag{9}$$

$$e\left(\xi_k^l,\xi_j^s,\xi_{jk}\right)^T=\xi_{jk}-\left(\xi_k^l\ominus\xi_j^s\right) \tag{10}$$

Compared with lidar only Cartographer's method, our method has added additional constraints, which may affect the sparsity of information matrix during system optimization. In this paper, we reduced the number of optimization times to avoid increased computation. Cartographer's pure localization depends on front-end odometry and back-end optimization. It is no longer effective to only use this method in the information degradation environment. However, after landmark constraint is obtained, the effect of back-end optimization can be improved. Therefore, in the degraded environment, we only carry out back-end optimization when landmark input is obtained to reduce the number of invalid back-end optimization. Refer to Algorithm 1 for the specific process.

IV. EXPERIMENTAL RESULT

In this section, we present the experimental results of Cartographer using ARTag as visual marker on UV disinfection robots. The platform used for this experiment is Aimi-Robot UVC, as shown in Fig. 3, which uses LS01B lidar to provide a scanning frequency of 10HZ and detection range of 25m, Generally, only 5m is used as the working range. The camera

Authorized licensed use limited to: HUNAN UNIVERSITY. Downloaded on April 09,2024 at 11:14:45 UTC from IEEE Xplore. Restrictions apply.

Algorithm 1: Improved back-end optimization strategies in localization

Input: Prior Node $\mathscr{X}_n = \{\Xi^m, \Xi^s, \Xi^l\}$, In pure location, each sensor gets ξ_l and ξ_s
Output: The optimized node $\mathscr{X}_{n+1}$

```
for i=1...N do
    ξ_s and ξ_l constructing new ξ_j^s, ξ_j^k and ξ_i^m
    if Obtained constraint of ξ_j^k then
        Optimize 𝒢 immediately // see Eq. (6)
        i = 0
    end
    if i>160 then
        Optimize 𝒢
        i = 0
    end
    i++
    Return 𝒳_{n+1}
end
```

use Realsense, which provide RGB images with resolution above 480p.

Fig. 3. Aimi-Robot UVC

We conducted mapping and pure localization experiments in long corridors of hospitals with unenclosed areas to demonstrate the effect of our method on laser information degradation environment. Finally, we compared the number of global optimizations used by different positioning methods.

A. Mapping

As shown in Fig. 4, it is the trajectory of the map we built in the corridor, and the environment of the map construction is a corridor 45m long and 2.5m wide. Four Artags with different digital information are placed on the path from the start point to the end point. Points a, b, c and d are marked on the yellow box in the figure. The sensor data in this process was recorded by rosbag. The subsequent experiments were based on the sensor data recorded this time. We installed a drip tube at the bottom of the robot, which dropped pigments. We collected 50 of these points and measured their positions to map the true trajectory of the robot in the corridor.

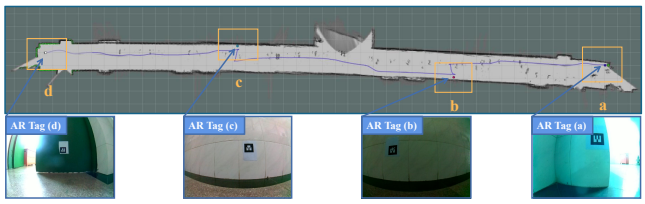

Fig. 4. The trajectory of mapping

As shown in the Fig. 5, it is the mapping results using Gmapping, Cartographer and Cartographer with ARTag respectively. It can be seen from the results that Gmapping produces map overlap in a long corridor environment, making the constructed map significantly shorter. Cartographer was significantly better built than Gmapping, and our method was consistent with Cartographer in building effect, while the boundaries of unenclosed areas were clearer.

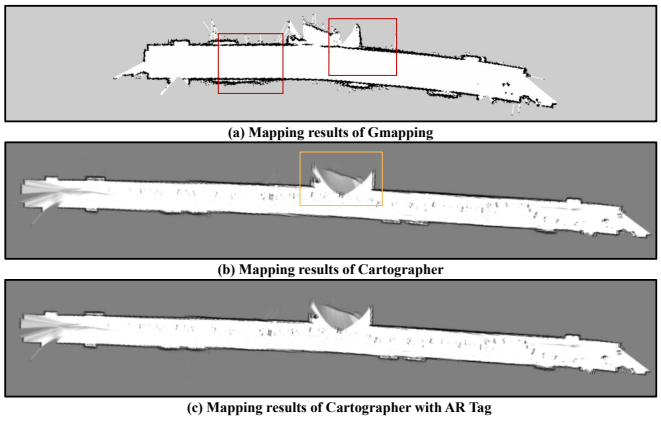

(a) Mapping results of Gmapping

(b) Mapping results of Cartographer

(c) Mapping results of Cartographer with AR Tag

Fig. 5. Comparison of mapping results

B. Localization

As shown in the Fig. 6, we used the map construction results of Cartographer with AR Tag as the map of our pure localization experiment. Three methods were used for positioning respectively. It can be seen that positioning errors occurred in long corridors and unenclosed environments when adaptive Monte Carlo localization (AMCL) [20] was used for positioning. In addition, when passing through the unclosed area between points b and c, the robot position jumps repeatedly and is constantly located to the position of the point b area in Fig. 6(a). Especially at the end of the trajectory, as shown in Fig. 6(b), the robot position has obviously drifted out of the map. However, due to the convergence of AMCL particles, The position of the robot is not corrected effectively. Cartographer also had a similar problem with AMCL when passing point b, that is, the position of the robot changed repeatedly, and the robot trajectory could not coincide with that of the mapping. Using our method, the robot quickly changes when it passes

Authorized licensed use limited to: HUNAN UNIVERSITY. Downloaded on April 09,2024 at 11:14:45 UTC from IEEE Xplore. Restrictions apply.

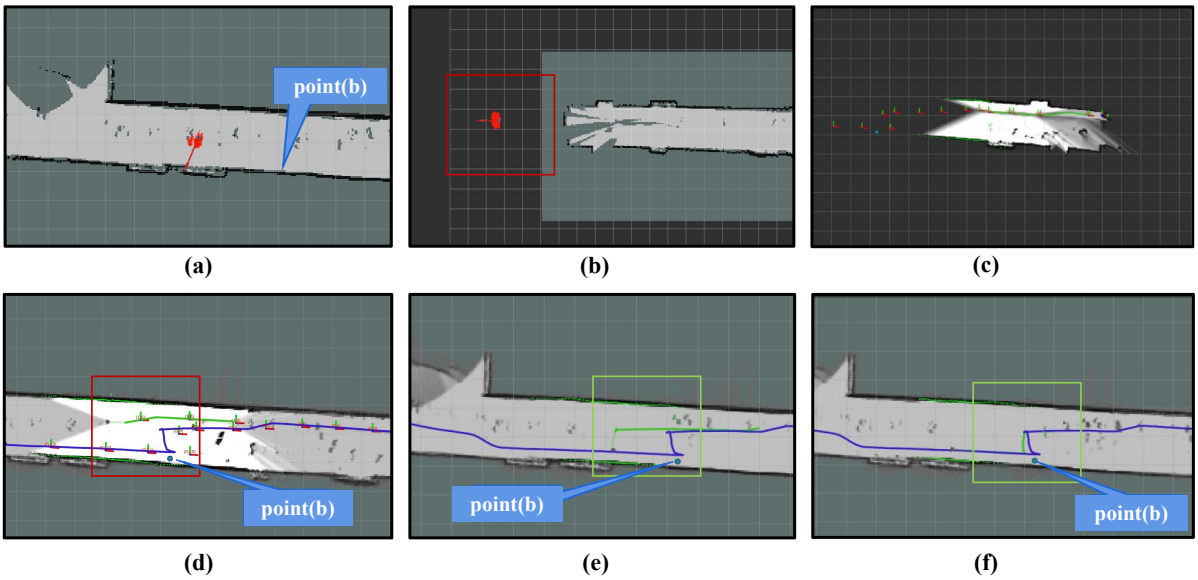

Fig. 6. The actual position of point b on the map has been marked in the figure. The red box in (a) shows the result of AMCL particle convergence. (b) is the localization of AMCL purely located at the end of the trajectory. (c) submap built for scan-matching in Cartographer pure localization. (d) is the matching result of Cartographer pure localization. The green track is the robot track during pure localization, and the blue track is the track during mapping. (e) is the trajectory of the Cartographer with ARTag about to pass point b for pure localization. (f) is the corrected trajectory of the Cartographer with ARTag after passing point b

point b, that is, its trajectory changes from Fig. 6(e) to Fig. 6(f), correcting the wrong positioning caused by laser degradation and making the trajectory of the robot coincide with the mapping, that is, the robot well matches its position in the map during repositioning. The Fig. 7 shows the trajectory curves of different methods in pure localization. Our method is closest to the real trajectory, Cartographer has obvious back and forth curves in several places due to laser degradation.

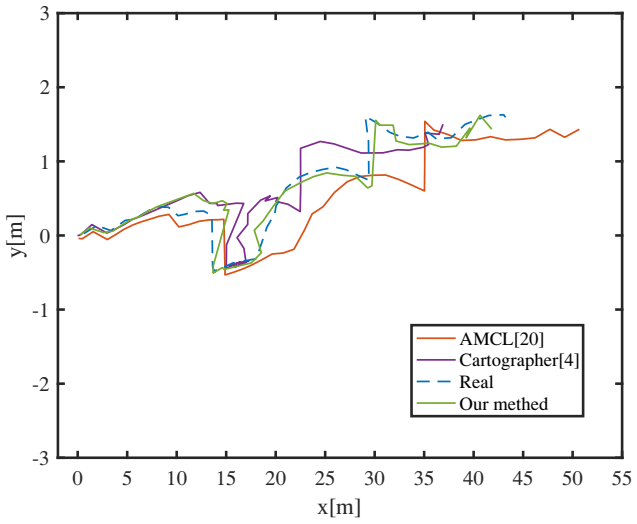

Fig. 7. Different methods of positioning curves

C. Analysis of Trajectory Error

The Table I records the positioning of the robot in the corridor map when the robot passes four points (Unit: m). The Table II statistics the positioning distance error of each point along the x direction (the corridor direction).

TABLE I
MEASUREMENT DATA

Test point	Real	AMCL [20]	Cartographer [4]	Our method
a	0.62	0.09	-0.02	0.23
b	13.64	14.88	15.24	13.68
c	29.04	35.05	22.47	30.12
d	43.22	51.28	37.52	41.80

TABLE II
ERROR DATA

Test point	AMCL [20]	Cartographer [4]	Our method
a	0.53	0.64	0.39
b	1.34	1.60	0.04
c	6.00	6.58	1.08
d	8.06	5.69	1.41

It can be seen that the positioning error of all methods is small at the beginning, but with the increase of the moving distance, the cumulative error gradually increases. Since AMCl particles have converged, errors continue to accumulate, and Cartographer cannot be effectively corrected by back-end optimization due to laser information degradation, resulting in errors approaching 6m when passing point c. However, our method after collecting information of visual markers, the back-end optimization effectively corrected the positioning errors. It can be clearly shown from the Fig. 8 that the error of our method is much smaller

Authorized licensed use limited to: HUNAN UNIVERSITY. Downloaded on April 09,2024 at 11:14:45 UTC from IEEE Xplore. Restrictions apply.

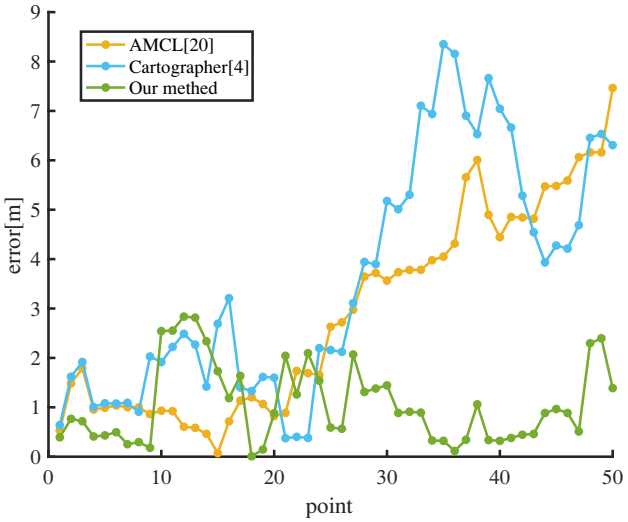

Fig. 8. Error curve

than that of the other two methods. The Table III shows that our strategy effectively reduced the number of global optimizations required for Cartographer's pure localization while still maintaining excellent positioning accuracy.

TABLE III
NUMBER OF BACK-END OPTIMIZATIONS

Test point	Cartographer [4]	Our method
a	1	1
b	13	4
c	29	9
d	40	13

V. CONCLUSIONS

In order to solve the problem of location failure caused by the degradation of indoor lidar information, this paper proposes a visual marker to assist location method based on graph optimization. The method is applied to the UVC Disinfection Robot for experiments. After the robot obtains landmark, the localization error of the robot is less than 1.5m by back-end optimization. Experiments show that the positioning error of our method is significantly lower than that of other mainstream methods in laser information degradation environment, and by counting the number of optimization times, the optimization frequency used in our positioning is triple lower than that of the ordinary method, but the positioning is more accurate.

In the future, we will explore a more elegant way to acquire landmark, as well as the sparsity problem after adding landmark constraints and conduct experiments in a larger scene to further improve the robustness of robot positioning and stability of computational quantity.

REFERENCES

[1] C. Cadena, L. Carlone, H. Carrillo, Y. Latif, D. Scaramuzza, J. Neira, I. Reid, and J. J. Leonard, "Past, present, and future of simultaneous localization and mapping: Toward the robust-perception age," *IEEE Transactions on robotics*, vol. 32, no. 6, pp. 1309–1332, 2016.

[2] G. Grisetti, C. Stachniss, and W. Burgard, "Improved techniques for grid mapping with rao-blackwellized particle filters," *IEEE transactions on Robotics*, vol. 23, no. 1, pp. 34–46, 2007.

[3] S. Kohlbrecher, O. Von Stryk, J. Meyer, and U. Klingauf, "A flexible and scalable slam system with full 3d motion estimation," in *2011 IEEE international symposium on safety, security, and rescue robotics*. IEEE, 2011, pp. 155–160.

[4] W. Hess, D. Kohler, H. Rapp, and D. Andor, "Real-time loop closure in 2d lidar slam," in *2016 IEEE international conference on robotics and automation (ICRA)*. IEEE, 2016, pp. 1271–1278.

[5] K. Konolige, G. Grisetti, R. Kümmerle, W. Burgard, B. Limketkai, and R. Vincent, "Efficient sparse pose adjustment for 2d mapping," in *2010 IEEE/RSJ International Conference on Intelligent Robots and Systems*. IEEE, 2010, pp. 22–29.

[6] M. Zhao, X. Guo, L. Song, B. Qin, X. Shi, G. H. Lee, and G. Sun, "A general framework for lifelong localization and mapping in changing environment," in *2021 IEEE/RSJ International Conference on Intelligent Robots and Systems (IROS)*. IEEE, 2021, pp. 3305–3312.

[7] J. Zhang, M. Kaess, and S. Singh, "On degeneracy of optimization-based state estimation problems," in *2016 IEEE International Conference on Robotics and Automation (ICRA)*. IEEE, 2016, pp. 809–816.

[8] A. Tourani, H. Bavle, J. L. Sanchez-Lopez, and H. Voos, "Visual slam: what are the current trends and what to expect?" *Sensors*, vol. 22, no. 23, p. 9297, 2022.

[9] P. Geneva, N. Merrill, Y. Yang, C. Chen, W. Lee, and G. Huang, "Versatile 3d multi-sensor fusion for lightweight 2d localization," in *2020 IEEE/RSJ International Conference on Intelligent Robots and Systems (IROS)*. IEEE, 2020, pp. 4513–4520.

[10] Y. Deng, Y. Shan, Z. Gong, and L. Chen, "Large-scale navigation method for autonomous mobile robot based on fusion of gps and lidar slam," in *2018 Chinese Automation Congress (CAC)*. IEEE, 2018, pp. 3145–3148.

[11] W. Zhen, S. Zeng, and S. Soberer, "Robust localization and localizability estimation with a rotating laser scanner," in *2017 IEEE international conference on robotics and automation (ICRA)*. IEEE, 2017, pp. 6240–6245.

[12] W. Zhen and S. Scherer, "Estimating the localizability in tunnel-like environments using lidar and uwb," in *2019 International Conference on Robotics and Automation (ICRA)*. IEEE, 2019, pp. 4903–4908.

[13] J. Xin, G. Xie, B. Yan, M. Shan, P. Li, and K. Gao, "Multimobile robot cooperative localization using ultrawideband sensor and gpu acceleration," *IEEE Transactions on Automation Science and Engineering*, vol. 19, no. 4, pp. 2699–2710, 2021.

[14] K. Michail, B. Cain, S. Carroll, A. Anand, W. Camden, and V. Nikolaos, "Fiducial markers for pose estimation," *Journal of Intelligent & Robotic Systems*, vol. 101, no. 4, 2021.

[15] Z. Zhang, "A flexible new technique for camera calibration," *IEEE Transactions on pattern analysis and machine intelligence*, vol. 22, no. 11, pp. 1330–1334, 2000.

[16] Q. Zhang and R. Pless, "Extrinsic calibration of a camera and laser range finder (improves camera calibration)," in *2004 IEEE/RSJ International Conference on Intelligent Robots and Systems (IROS)(IEEE Cat. No. 04CH37566)*, vol. 3. IEEE, 2004, pp. 2301–2306.

[17] M. Fiala, "Artag, a fiducial marker system using digital techniques," in *2005 IEEE Computer Society Conference on Computer Vision and Pattern Recognition (CVPR'05)*, vol. 2. IEEE, 2005, pp. 590–596.

[18] G. Grisetti, R. Kümmerle, C. Stachniss, and W. Burgard, "A tutorial on graph-based slam," *IEEE Intelligent Transportation Systems Magazine*, vol. 2, no. 4, pp. 31–43, 2010.

[19] Z. Li, G. Li, X. Wu, Z. Kan, H. Su, and Y. Liu, "Asymmetric cooperation control of dual-arm exoskeletons using human collaborative manipulation models," *IEEE Transactions on Cybernetics*, vol. 52, no. 11, pp. 12 126–12 139, 2022.

[20] S. Thrun, "Probabilistic robotics," *Communications of the ACM*, vol. 45, no. 3, pp. 52–57, 2002.

Authorized licensed use limited to: HUNAN UNIVERSITY. Downloaded on April 09,2024 at 11:14:45 UTC from IEEE Xplore. Restrictions apply.